Vortex Induced Vibration of an Elastically Mounted Circular Cylinder with Forced Rotataions

MARINE 2011

Zhiyong. Huang*, Carl. M. Larsen*†

* Centre for Ships and Ocean Structures, 7050, Trondheim, Norway
e-mail: zhiyong.huang@ntnu.no

† Department of Marine Technology, Norwegian University of Science and Technology, 7050, Trondheim, Norway
Email: carl.m.larsen@ntnu.no

Key words: Vortex-induced vibrations; Rotation; Circular cylinder; Wake structures; Hydrodynamic forces.

Summary: Flow over an elastically mounted circular cylinder with forced rotation is numerically studied in this paper. The cylinder vibrates in in-line and cross-flow directions, and the rotating speed is constant. Reynolds number was fixed at 5000, and the shear stress transport *k-w* model was used to simulate turbulence in the flow. The effect on the response, hydrodynamic force and wake structure from rotation are extensively studied. Higher harmonic fluid forces and the trajectories of the cylinder motions are also investigated under various reduced velocities.

1 INTRODUCTION

Vortex-induced vibrations (VIV) have attracted attention in the last two decades because this response can cause large fatigue damage in engineering structures such as bridges, chimneys, marine risers and pipelines. Progressive achievements in the fundamental VIV mechanism and industry applications are summarized in the review papers by Berman (1998), Sarpkaya (2004), Williamson and Govardhan (2004, 2008) and Lie and Larsen (2006).

Research work on unsteady flow passing an oscillating cylinder can be classified in to two categories depending on the motion of the cylinder. In the first category, the cylinder can oscillates in in-line or transverse direction with respect to the free stream. Studies on transverse oscillation can be found in Feng (1968), Gopalkrishnan (1993), Khalak and Williamson (1996, 1999), Govardhan and Williamson (2000, 2002), while Wootton et al. (1972), King and Johns (1973) and Aronsen (2007) studied in-line oscillations. Recently, the combination of in-line and cross flow oscillation becomes a major concern since fatigue damage from IL may exceed CF; see Baarholm et al. (2006). In the second category, the cylinder can rotate around its own axis in the flow, and this rotatinal is known to give some drag reduction. Experimental work on rotating cylinders in uniform flow was investigated by Wu (1990), Filler et al. (1991), Tokumaru and Dimotakis (1991), Dennis et al. (2000) and Cheng et al. (2001). It is found that the vortex shedding sycchronised with the cylinder motion when the rotational frequency is close to the the vortex shedding frequency from a stationary cylinder. Another interesting finding is that the rotational speed at very large magnitudes can produce significant reduction in drag force when the rotational frequency is out of the knock-in stage.

This paper is with an attempt to investigate the combination of these two category movements; i.e, the cylinder can vibrate freely in in-line and cross flow directions, while a constant rotating speed takes place. The motivation of this work is to study the rotating effect on the results of motions, fluid forces and wake structures.

2 NUMERICAL METHOD

The Reynolds-averaged equations, which presents the governing equations for two-dimensional flow motion, are solved by using a finite-volume method in combination with an *SST* k-ω turbulence model . The implicit first-order scheme was used for the unsteady term and the SIMPEC algorithm for the pressure-velocity coupling equations. A second order scheme was applied for the k and ω transport equations, and for the convection and diffusion terms.

The non-dimensional governing equations for the freely vibrating cylinder are listed as follows:

$$\frac{d^2Y}{d\tau^2}+\frac{4\pi\zeta}{U^*}\frac{dY}{d\tau}+\frac{4\pi^2}{U^{*2}}Y=\frac{2C_L}{\pi m^*} \quad (1)$$

$$\frac{d^2X}{d\tau^2}+\frac{4\pi\zeta}{U^*}\frac{dX}{d\tau}+\frac{4\pi^2}{U^{*2}}X=\frac{2C_d}{\pi m^*} \quad (2)$$

where $Y=y/D$, $X=x/D$ are the normalized displacements in CF and IL directions respectively, and D is the cylinder diameter. ζ is the structural damping ratio, $m^*=m/m_d$ is the mass ratio and $U^*=U_f/(f_n D)$ is the reduced velocity. f_n is the nature frequency in still water. C_L and C_d are the non-dimensional lift and drag forces respectively. A forth-order Runge-Kutta algorithm is used to integrate Eqs.(1-2) in the time domain. Once the two equations (1-2) are resolved, the updated displacement and velocity are used to control the movement of the cylinder at each time-step.

A forced rotating speed is added to the free vibrating cylinder, and the non-dimensional rotating ratio can be expressed as:

$$r=\omega D/\left(2U_f\right) \quad (3)$$

where ω is the rotating speed. In this paper, three rotating ratios at r=0, 0.1 and 0.25 are calculated to investigate the rotating effect on responses, hydrodanamic forces and wake structures.

The Reynolds number $\mathrm{Re}=U_f D/\upsilon$ is fixed at 5000 for all the simultations in this paper, and the mass ratio $m^*=2.6$. A list of key parameter in the present simulations is shown in Table 1.

	Simulated parameters
Reynolds number Re	5000
Flow velocity U_f	0.13 m/s
Cylinder diameter D	38 mm
Mass ratio m^*	2.6
Rotating ratio r	0-0.25
Damping ratio ς	0.36%

Table 1: Key parameters in the present simulations

Fig 1 (a) shows the physical model of an elastically mounted cylinder with a rotating speed, and Fig. 1 (b) presents the grid that has been applied in the present study. The flow domain has a size of $45D\times30D$ in the x and y directions, respectively, and the cylinder centre is located at a distance of $15D$ away from the front borderline. Dynamic mesh strategy is applied in order to obtain a good numerical performance for the analysis of the moving cylinder. The density mesh around the cylinder surface goes rigidly with the cylinder, while the mesh outside is deformed according to the movement of the inner mesh. The Lagrangian-Eulerian method is applied to accommodate the cylinder motion. The varying position and velocity of the cylinder at each time-step are initially calculated by solving the equations (1-2); the cylinder surface and the moving grid are then updated based on the new position; the Navier-Stokes equations are finally solved based on the new mesh. Grid tests give a total of 14150 mesh points for the computational model.

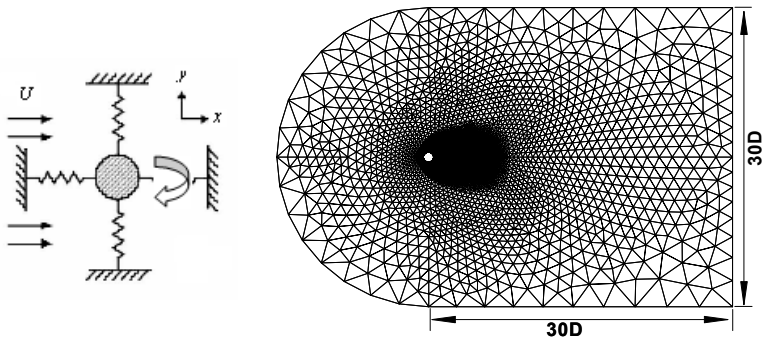

(a) (b)

Figure 1. (a) Model of an elastic mounted cylinder with forced rotations, and (b) computational grid.

The inlet velocity is set at the left borderline, and the flow goes from left to right. The outlet pressure is used for the right borderline, and there are symmetric boundary conditions for the top and the bottom borderlines. The no-slip boundary condition is applied on the cylinder surface. The non-dimensional time-step is set to 0.002 based on $\tau = U_f * dt / D$ (dt is the time step) and a minimum of 500 time steps are used for every cycle of cylinder motions. More than 40 rotation periods are analyzed for each case, and the calculation of hydrodynamic coefficients is based on the time history for the last 20 oscillating cycles when the fluid forces have become periodic.

3 RESULTS AND DISCUSSION

The respons of the vibrating cylinder without forced rotation are initially investigated and compared with experimental results from Jauvtis and Williamson (2004); see Fig 2. The CF response presents three branches; i.e, initial branch, upper branch and lower branch. The peak point reaches $A_y^* = 1.08$, and it moves to the lower branches at reduced velocity $U^* = 5.4$. However, the peak response arrives at $A_y^* = 1.5$ at $U^* = 8.4$ within the supper-upper branch in the experiments. This discrepancy is most probably caused by the difference in Reynolds number between the present simulation and the experiment. The Reynolds number is fixed at Re=5000 for all of simulations in this paper, while it is gradually increased from 2000 to 13000 in the experiment. Another potential reason for the discrepancy could be related to the use of a two-dimensional model which is unable to reproduce the effect of the three-dimendional flow motion.

Fig 2 (b) presents the comparison of in-line responses from the present simulations to the experimental results form Jauvtis and Williamson (2004). It is clear that the in-line response is observed as two dominated regions, where the first region is within the lower reduced velocity range of $U^* \in [1.8, 3.4]$; and the second in-line region is from $U^* = 4.2$ to 5.8 which is corresponding to the upper branch for CF response. The peak IL response $A_x^* = 0.2$ is observed in the second region which follows the same tendency of the experimental results. However, The peak value of IL response is lower than the experimental results , and the reasons are most likely the same as discussion for CF respons.

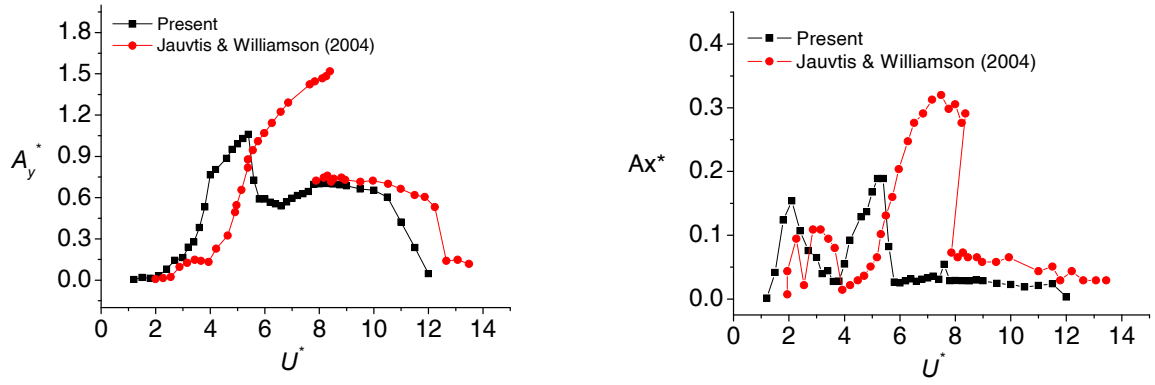

(a) (b)

Figure 2. Response amplitude A_y^* and A_x^* are plotted with normalized velocity U^*, here the cylinder is free to response in CF and IL direction without rotating speed; i.e, r=0.

The comparison of IL and CF response generated from three rotating ratios are shown in Fig 3 (a) and Fig 3 (b) respectively. The peak CF response is increased when the cylinder is with r is increased from r=0 to 0.1. However, the increasing trend of CF response is changed with an increasing rotating speed, and a slight decrease in CF response is observed when the rotating ratio is increased from r=0.1 to 0.25. It is found that the rotating speed do not affect the initial branch too much, but a wilder lock-in region is observed with a higher rotating speed for the upper and lower branches. Two IL response regions are clearly observed, and the peak point is located in the second region for the two rotation cases.

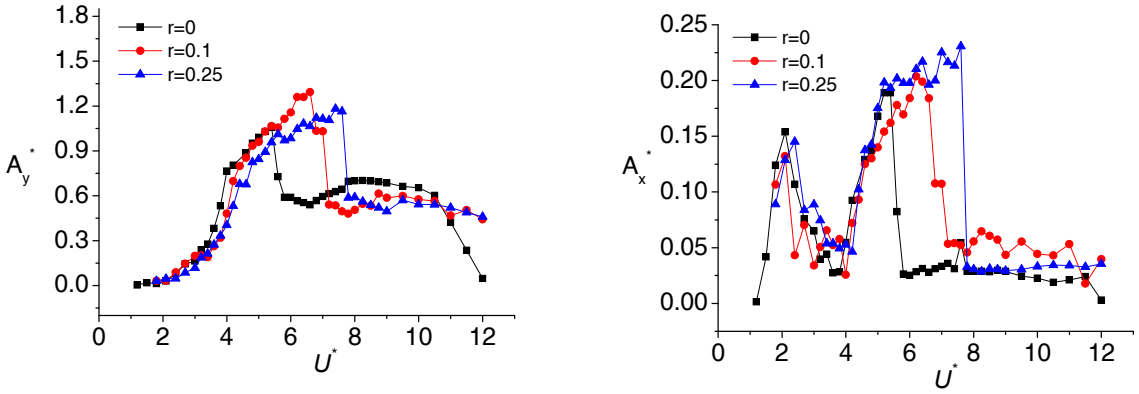

(a) (b)

Figure 3. Comparison of response amplitude A_y^* and A_x^* for three rotating ratios.

The averaged IL displacement variation with the reduced velocity is shown in Fig 4. Even though IL response are close to each other for the three rotating ratios (see Fig 3 (b)); the averaged IL displacement is with a large increasement when the rotating speed is increased. When the rotating cylinder leaves the lock-in region, a sharp decrease of the averaged IL displacement occurs. A sharp decrease of the CF response from upper branch to lower branch is also seen from Fig 3 (a).

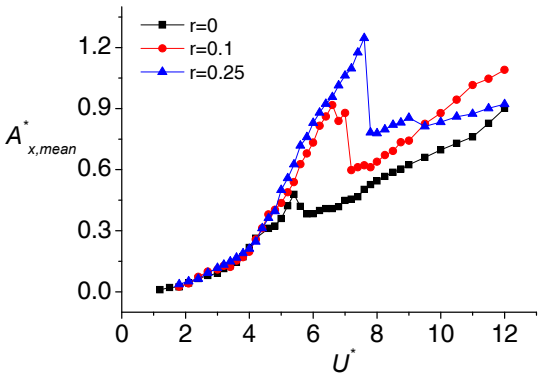

Figure 4. Comparison of averaged in-line displacement $A^*_{x,mean}$ for three rotating ratios.

A selected time history of the responses and fluid forces for three reduced velocities in r=0 are shown in Fig 5. The lift force and CF response are found to be close to sinusoidal at the reduced velocity $U^* = 3.6$ in the initial branch. When the reduced velocity is increased to $U^* = 5.4$, the lift force is seen to contain larger order frequency compounds while the motion remains harmonic. An out of phase phenomenon is observed for the reduced velocity arrives at the lower branch for $U^* = 10.0$ A similar conclusion has been found in Aronsen et al. (2008) in which the cylinder is forced to oscillate with pure sinusoidal CF and IL motions, but non-sinusoidal fluid forces are produced in their experiments. This finding is further confirmed in a three dimensional numerical study by Huang et al. (2009). The power spectrum analysis of the time-history of hydrodynamic forces reveals that the non-sinusoidal profiles are related with higher order force components occurring at multiples of the oscillation frequencies. The CF force components are related with odd numbers (1,3,5), while even numbers (2,4,6) dominate for the IL force components. The third order force component in the lift force can be inferred from the phase plots between lift force and CF displacement; as seen from the right column of Fig 5.

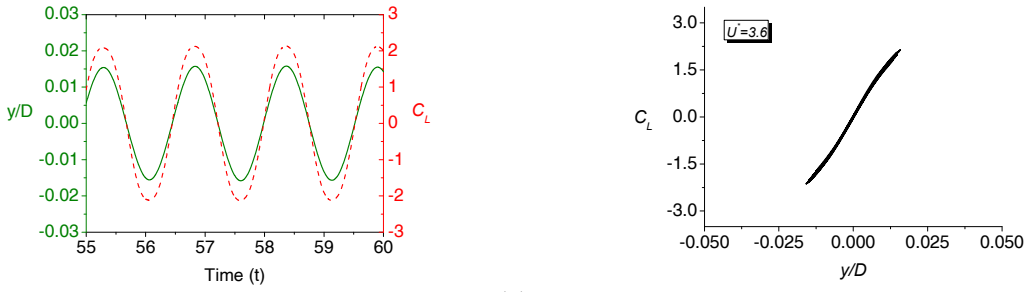

(a)

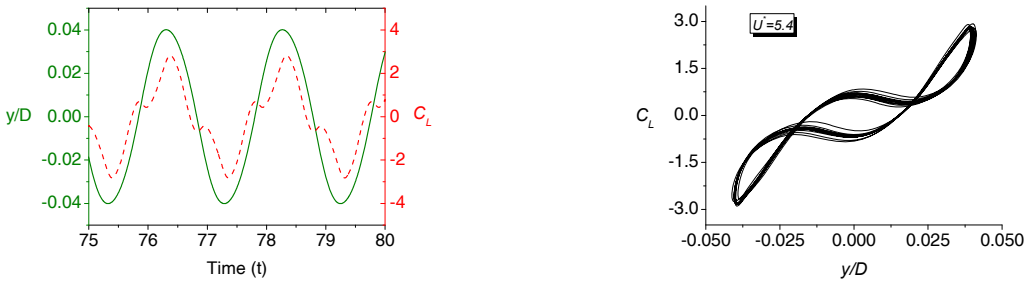

(b)

To be continued

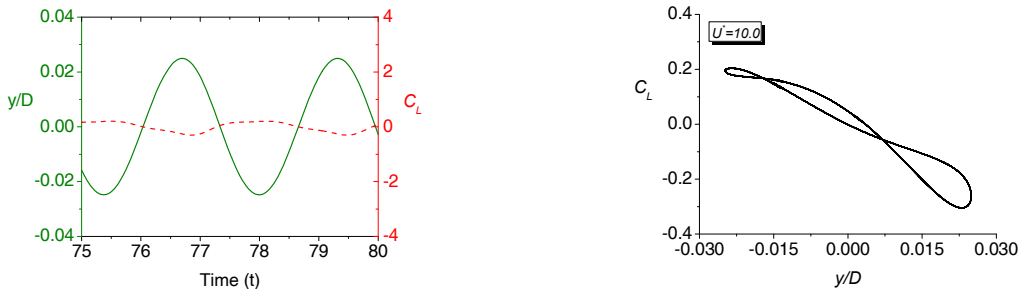

(c)

Figure 5. The first column presents time history, and the second comumn shows phase plot between CF displacement and lift force. Here r=0. (a) $U^*=3.6$,(b) $U^*=5.4$,(c) $U^*=10.0$.

Time histories of CF displacement and lift force at three selected reduced velocities for r=0.1 and r=0.25 are shown in Fig 6 and Fig 7 respectively. As the cylinder is given a rotating speed, it is found that the displacement and lift forces are no longer observed as sinusoidal profiles within the initial branches. However, similarites such as high order force components, phase shift phenomenon can be observed for the upper and lower branches. The phase plot between lift force and CF displacement turns to be irregular and complicated compared to the results in the r=0 case.

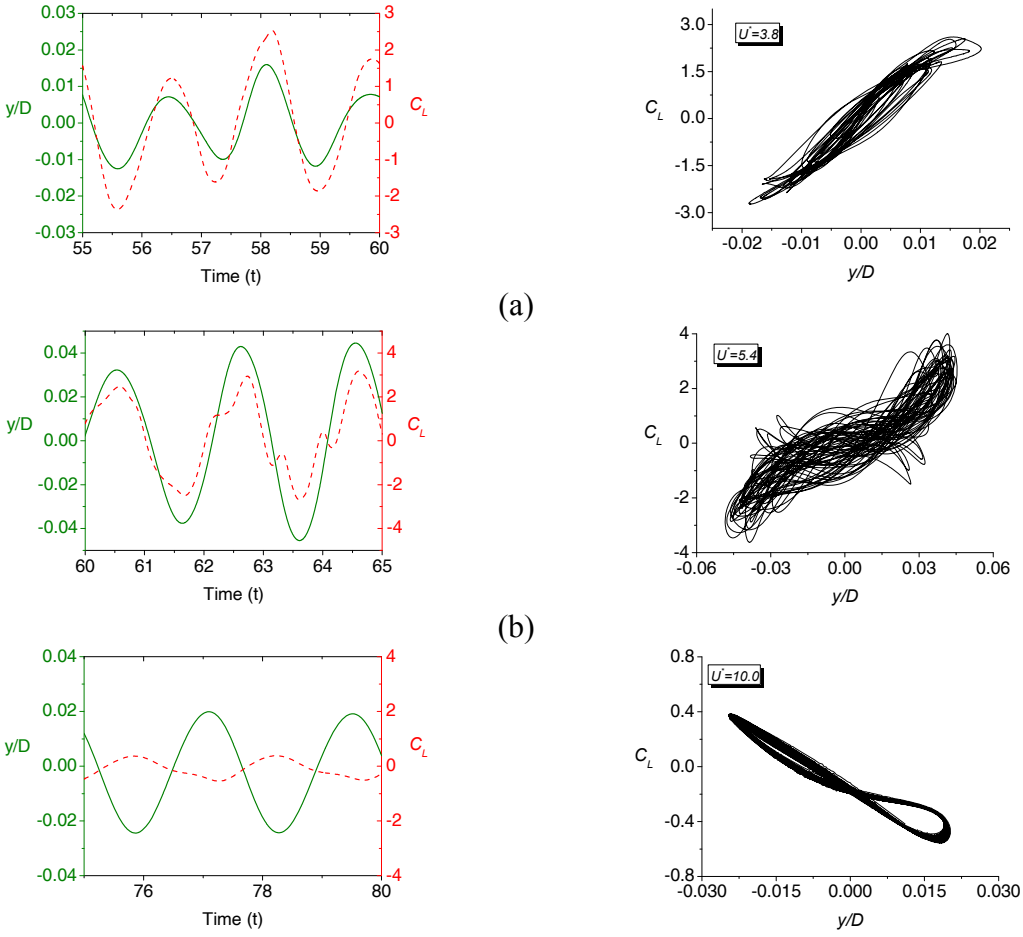

(a)

(b)

(c)

Figure 6. Time history of CF displacement and lift force for r=0.1;. (a) $U^*=3.8$,(b) $U^*=5.4$,(c) $U^*=10.0$.

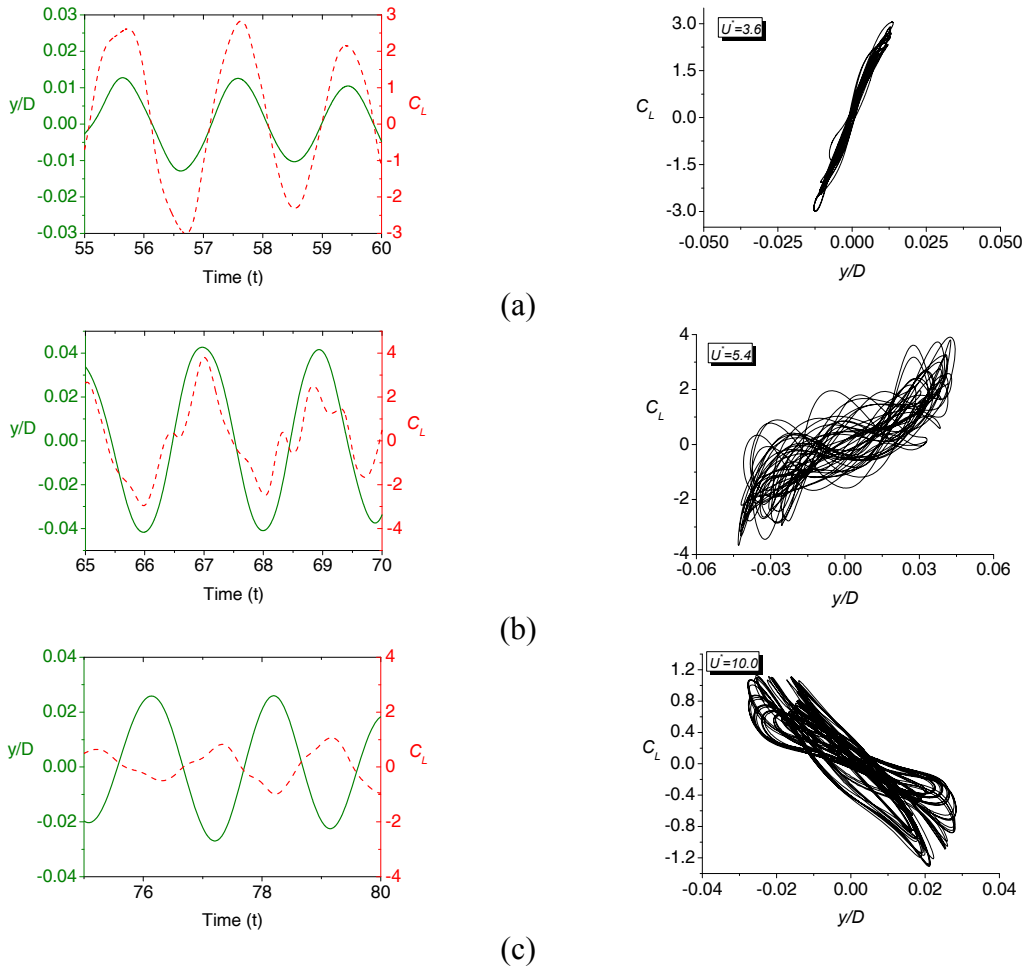

Figure 7. Time history of CF displacement and lift force for r=0.25;. (a) $U^* = 3.6$,(b) $U^* = 5.4$,(c) $U^* = 10.0$.

Fig 8 presents the comparison of phase plots between the non-dimensional CF and IL displacement. The first row shows the results from r=0; and the second row is from r=0.25. A typical figure of "8" moving trajectory of the cylinder is clearly observed for r=0. Those profiles follow similar shapes found in the experiments; referring to Fig 14 in Jauvtis and Williamson (2004). However, the moving trajectory becomes more irregular and complicated when the cylinder is with a rotating speed, and no periodic figure of "8" can be observed for the case of r=0.25.

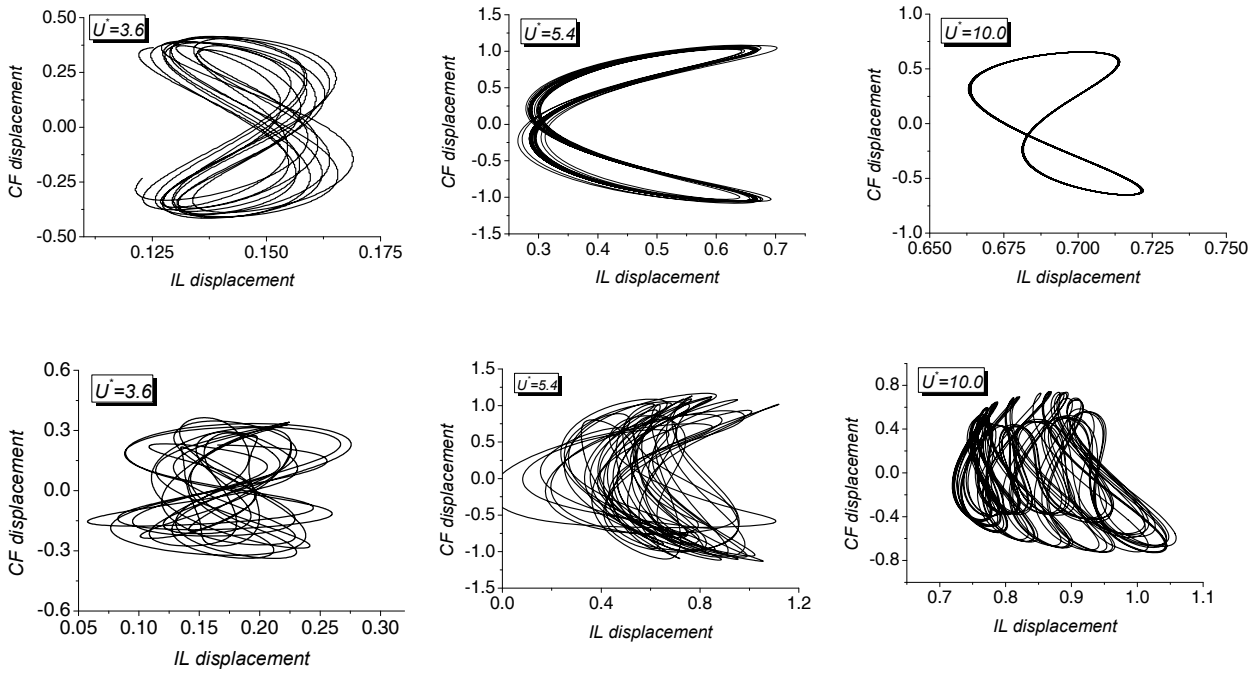

Figure 8. Phase plots between CF and IL displacements for r=0 in the first row; the second row for r=0.25.

It is known from previous experiments by Khalak and Williamson (1996, 1999) and Govardhan and Williamson (2000, 2002) that three classical wake structures can be produced by an elastically mounted cylinder without forced rotations; i.e., the 2S mode for initial branch, 2P modes for upper and lower branches. Here, 2S means two single vortices shed for each cycle; 2P means two pairs of vortices shed each cycle. Fig 9 presents four frames of the 2S mode during one cycle observed in the initial branch at $U^* = 2.7$ for r=0. The position of the cylinder can be seen from the marked number corresponding to the time history of CF displacement in the right plot. The lift and drag forces are also included in the same plot. It is seen the lift force and CF displacement is in phase with each other in the initial branch. An phase shift of 180 degrees for wake structure is clearly observed between position 1 and 3; i.e; a red vortex (anti-clockwise) is about to shed in the lower part of the cylinder, while a blue vortex (clockwise) is shed into the wake on the upper of the cylinder.

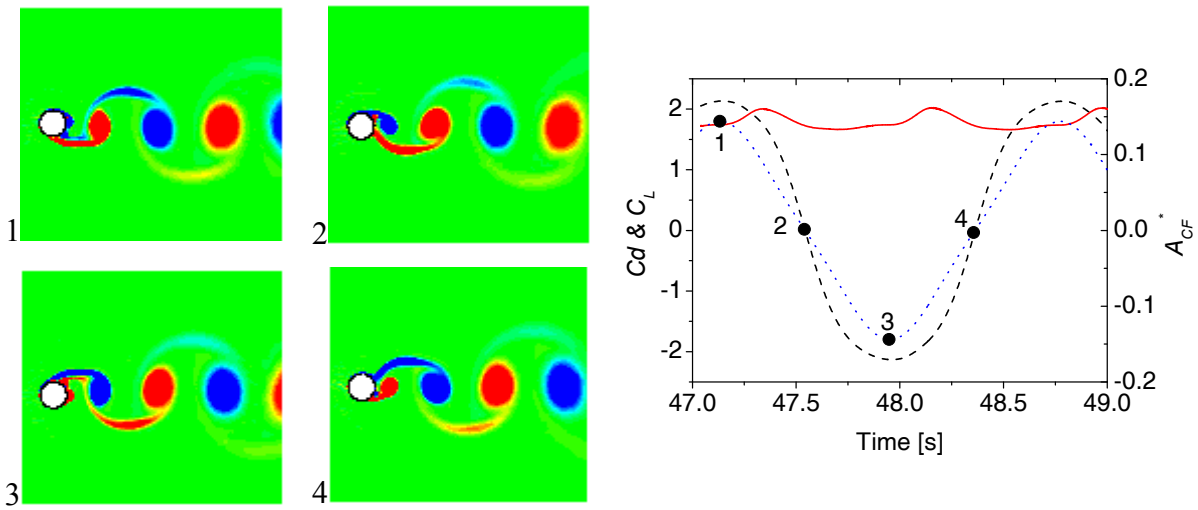

Figure 9. 2S wake mode in the initial branch at $U^* = 2.7$ for r=0. The solid line presents drag force; dash line for lift force; dot line for CF response.

The 2P mode for upper branch is presented in Fig 10. This 2P mode consists two pairs of vortices shed each cycle, and the energy of one vortex in the pair is much greater than the other one. From the time history of lift force and displacement, it is clearly observed that the CF displacement and force have opposite phase. i.e.; the CF displacement has its maximum positive value at position 1; while the lift force is at its largest negative value. The minimum value of CF displacement is observed at position 3; while the lift force comes to its maximum value.

The 2P mode for lower branch also includes two pairs of vortices shed each cycle. However, each vortex in the pair has equal energy; as shown in Fig 11. The displacement amplitude for lower branch is decreased compared to the upper branches, and the magnitude of lift force is also significantly decreased since this condition is outside the lock-in region.

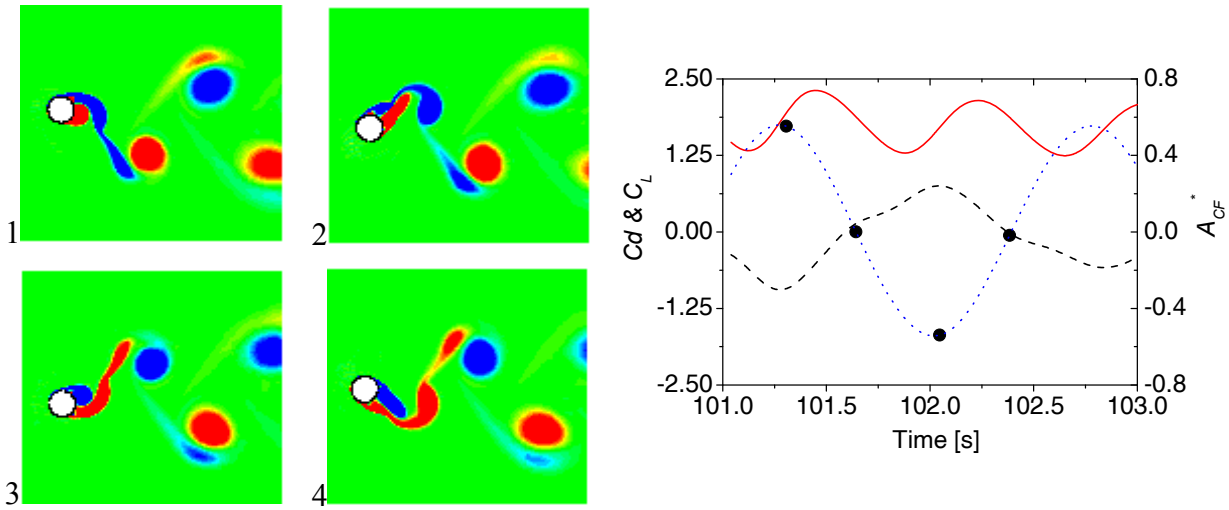

Figure 10. 2P wake mode in the upper branch at $U^* = 5.8$ for r=0. The solid line presents drag force; dash line for lift force; dot line for CF response.

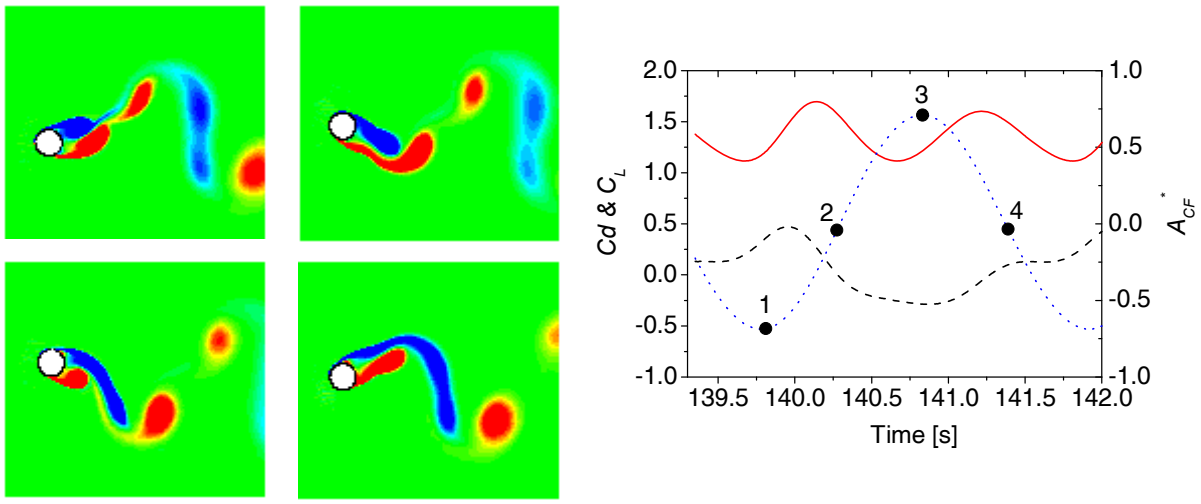

Figure 11. 2P wake mode in the lower branch at $U^* = 8.0$ for r=0. The solid line presents drag force; dash line for lift force; dot line for CF response.

When a forced rotation of the cylinder is applied, the wake structures is totally changed. Fig 12 presents wake structures for r=0.25 at reduced velocity $U^*=2.7$. Two co-rotating vortices are observed (i.e., 2C mode) close to the cylinder; but the wake structure finally turns to 2S mode when the two co-rotating vortices have merged into one big vortex in far wake. The time histories of lift and drag forces, CF displacement become more irregular than the case for the cylinder without rotating speed.

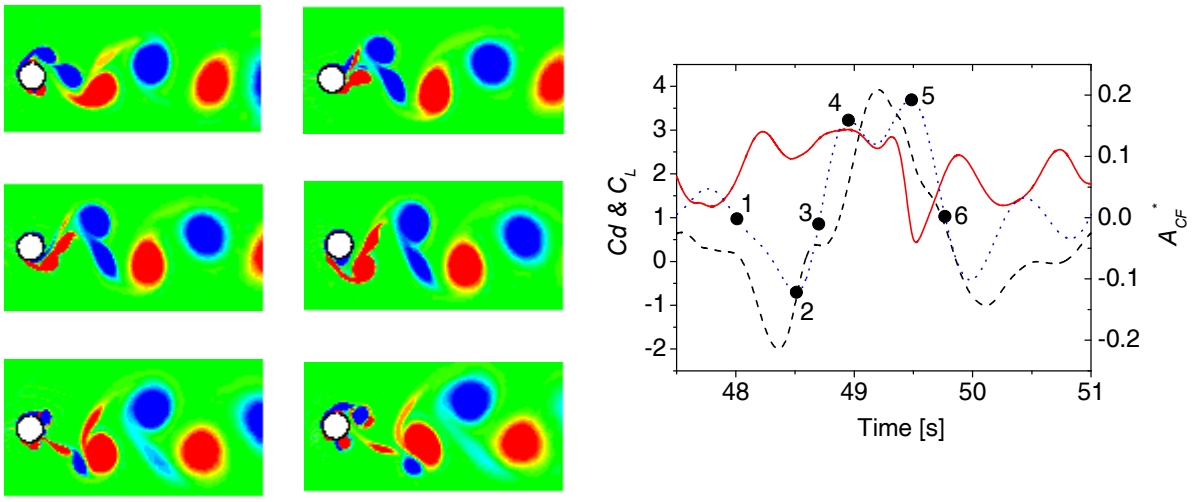

Figure 12. Wake structure for U^*=2.7, r=0.25. The solid line presents drag force; dash line for lift force; dot line for CF response.

Fig 13 presents the wake structures for U^*=8.0 and the rotating ratio is r=0.25. As discussed in the previous section, a 2P mode in captured for U^*=8.0 at lower branch when no rotating speed is applied. However, as the rotating speed is added, the wake structure keeps a 2P style, but it is close to the 2P mode corresponding to the upper branch; i.e., the energy of each vortex within one pair is no longer equivlent.

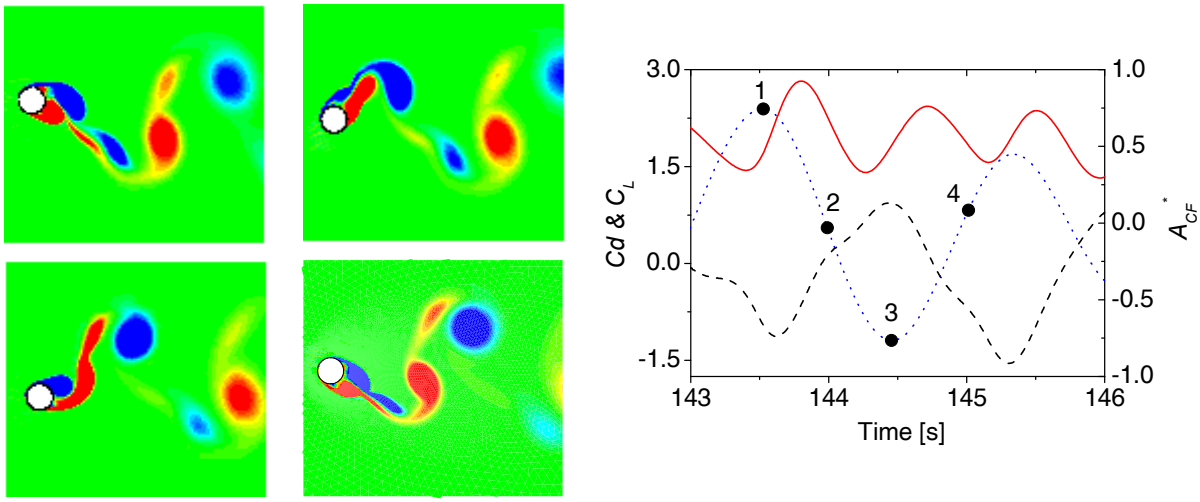

Figure 13. Wake structure for U^*=8.0, r=0.25. The solid line presents drag force; dash line for lift force; dot line for CF response.

4 CONCLUSIONS AND FUTURE WORK

Vortex induced vibrations of an elastically mounted cylinder with a forced rotating speed are extensively investigated in the present numerical simulations. The rotating speed effect from two rotating ratios r=0.1 and r=0.25 are compared with equivalent case without rotation. For the cylinder with a rotating speed, it is found that CF response is increased by 10% to 12%, and a wider lock-in region can be observed for increasing of rotating speed. The peak value of IL response and averaged IL displacement are also increased with increasing rotating speed. Higher order force components are found in the time history of lift force and the phase plots between CF displacement and lift forces. This phase plot becomes more irregular and complex when the rotating speed is added to the cylinder. A typical figure of "8" trajectory is observed for the cylinder without rotation, while no periodic pattern can be obtained as the cylinder rotates. Three wake patterns named 2S and 2P modes are reproduced corresponding to initial, upper and lower branches. For rotating cylinder cases, a transformed wake pattern similar to a 2S mode is produced at lower reduced velocities, and the 2P mode is observed for higher reduced velocity ranges corresponding to the lower branch.

REFERENCES

1 Aronsen, K.H. "An Experimental Investigation of In-line and Combined In-line and Cross-flow Vortex Induced Vibrations." Ph.D. Thesis, Department of Marine Structures, NTNU, Norway. (2007).

2 Aronsen, K.H., Huang, Z., Skaugset, K.B., Larsen, C.M. Interaction between IL and CF VIV- on the importance of orbital direction. (2010). (unpublished).

3 Baarholm, G.S., Larsen, C.M., Lie, H., On fatigue damage accumulation from in-line and cross-flow vortex-induced vibrations on risers, Journal of Fluids and Structures, 22, 109-127. (2006).

4 Bearman,P.W. , Developments in the understanding of bluff body flows , Jsme International Journal Series B-Fluids and Thermal Engineering , 41, 103-114. (1998).

5 Cheng, M., Chew, Y. T. and Luo, S. C., Numerical investigation of a rotationally oscillating cylinder in mean flow, Journal of Fluids and Structures, Vol. 15, 981-1007 (2001).

6 Dennis, S., Nguyen, P. and Kocabiyik, S, The flow induced by a rotationally oscillating and translating circular cylinder, J. Fluid Mech., 407, 123-144, (2000).

7 Feng, C.C., The measurement of vortex induced effects in flow past stationary and oscillating circular and d-section cylinders. Master's Thesis, Department of Mechanical Engineering, University of British Columbia, Canada. (1968).

8 Filler, J.R., Marston, P.L. and Mih, W.C., Response of the shear layers separating from a circular cylinder to small-amplitude rotational oscillations. Journal of Fluid Mechanics 231, pp. 481–499. (1991).

9 Gopalkrishnan, R. Vortex induced forces on oscillating bluff cylinders. Ph.D. Thesis, Department of Ocean Engineering, MIT, Cambridge, MA, USA. (1993).

10 Govardhan, R., Williamson, C.H.K. Modes of vortex formation and frequency response for a freely vibrating cylinder. Journal of Fluid Mechanics. 420, pp.85-130. (2000).

11 Govardhan, R., Williamson, C. H. K. Resonance forever: existence of a critical mass and an infinite regime of resonance in vortex-induced vibration. Journal of Fluid Mechanics, 473, pp. 147-166. (2002).

12 Huang, Z.Y., Larsen, C.M., Cui, W.C. three dimensional LES study on a forced oscillating circular cylinder following the Figure of Eight movement. 5th International conference on hydro-elasticity in marine technology, Southampton, UK. (2009).

13 Lie, H. and Larsen, C.M. Vortex induced vibrations of deepwater risers and pipelines - review of model test results. 4th International conference on hydro-elasticity in marine technology, Wuxi,China. (2006).
14 Khalak, A., Williamson, C.H.K. Dynamics of a hydro-elastic cylinder with very low mass and damping. Journal of Fluids and Structures 10, pp.455-472. (1996).
15 Jauvtis, N., Williamson, C.H.K. The effect of two degrees of freedom on vortex-induced vibration at low mass and damping, Journal of Fluid Mechanics 509.pp. 23–62. (2004).
16 Khalak, A., Williamson, C.H.K. Motions, forces and mode transitions in vortex-induced vibrations at low mass-damping. Journal of Fluids and Structures 13, pp.813-851. (1999).
17 King, R., Prosser, M.J, and Johns. D.J. On vortex excitation of model piles in water. Journal of Sound and Vibration, 29,169-188. (1973).
18 Sarpkaya, T. A critical review of the intrinsic nature of vortex-induced vibrations. Journal of Fluids and Structures 19, pp.389-447. (2004).
19 Tokumaru, P. T. and Dimotakis, P. E., Rotary oscillation control a cylinder wake. Journal of Fluid Mechanics 224, pp. 77–90. (1991).
20 Williamson, C.H.K. and Govardhan, R. Vortex-induced Vibrations. Annual Review of Fluid Mechanics, 36, 413-455. (2004).
21 Williamson, C.H.K. and Govardhan, R. A brief review of recent results in vortex-induced vibrations, Journal of Wind Engineering and Industrial Aerodynamics, 96, 713–735. (2008).
22 Wu, J.M. On oscillating shear layer excitation of a cylinder. Engineering Science, Fluid Dynamics, World Scientific Publishing Company, Singapore p. 341–351. (1990).
23 Wooton, L.R., Warner, M.H., Sainsbury, R.N., Cooper, D.H. Oscillations of piles in marine structures. A resume of full-scale experiments at Immingham. CIRIA Technical Report 41, (1972).